Two-photon absorption enhancement by the inclusion of saddle curvature in distorted nanographene ribbons

Silvia Castro-Fernández,[a]¶ Carlos M. Cruz,[a]¶ Inês F. A. Mariz,[b] Irene R. Márquez,[a] Vicente G. Jiménez,[a] Lucía Palomino-Ruiz,[a] Juan M. Cuerva,[a] Ermelinda Maçôas*[b] and Araceli G. Campaña*[a]

Abstract: A new family of distorted ribbon-shaped nanographenes was designed, synthesized and their optical and electrochemical properties were evaluated, pointing out an unprecedented correlation between their structural characteristics and the two photon absorption (TPA) responses and electrochemical band gaps. Three nanographene ribbons have been prepared: a seven-membered ring containing nanographene presenting a tropone moiety at the edge, its full-carbon analogue and a purely hexagonal one. We have found that the TPA cross-sections and the electrochemical band gaps of the seven-membered ring containing compounds are higher and lower, respectively, than those of the fully hexagonal polycyclic aromatic hydrocarbon (PAH). Interestingly, the presence or absence of the electron withdrawing group, barely changes these parameters compared to those of the nanoribbon without the heptagon.

The intense research carried out in the field of nanographenes is highly driven by their potential applications.[1] A countless number of spherical, tubular, ribbon and other original shaped polycyclic aromatic hydrocarbons (PAHs) have been synthesized and tested for applications as sensors, catalysis or electrochemical systems, among others.[2] The origin of such versatile capabilities is the combination of their 2D aromatic network with the perturbations caused by the introduction of defects.[3]

Particularly inspiring are the new developments based on the optical properties of nanographenes and related materials.[4] Nanographenes have been recently introduced as a new class of fluorophores for super-resolution fluorescence microscopy,[4c] graphene quantum dots (GQDs) and carbon dots (CDs) have been extensively explored in photonic and optoelectronic applications,[4d] and their non-linear optical (NLO) response has been applied in multiphoton imaging and sensing.[4e]

Despite the reports on CDs and GQDs with two photon absorption (TPA) cross-sections larger than other organic dyes and semiconductors quantum dots,[5] the origin of their photoluminescence mechanisms is still to be clarified.[6] Much of the ambiguity in this field is due to the heterogeneity of the produced samples. Thus, the study of well-defined nanographene molecules is mandatory to understand how structural defects of graphene related materials define their properties.

Nanographenes present a highly delocalized π-conjugation, which makes them good candidates for the development of well-defined NLO materials,[7] and their structures can be easily tuned and studied.[8]

Materials presenting two-photon absorption (TPA) response are of tremendous interest in different fields including nanomedicine and biomedical research, because the use of near-infrared light offers the possibility of light actuation at larger penetration depths (deeper tissue penetration) and the nonlinear dependence of the excitation offers intrinsic localization in space.[9]

There are two critical structural requirements for a compound to present a high TPA cross-section: a conjugated backbone and an excited charge-transfer process usually promoted by the functionalization of the conjugated core with electron donor (D) and/or acceptor (A) groups; for example, a D-π-A-type chromophore.[7,10] It has been demonstrated that the enlargement of the aromatic surface leads to a higher TPA response.

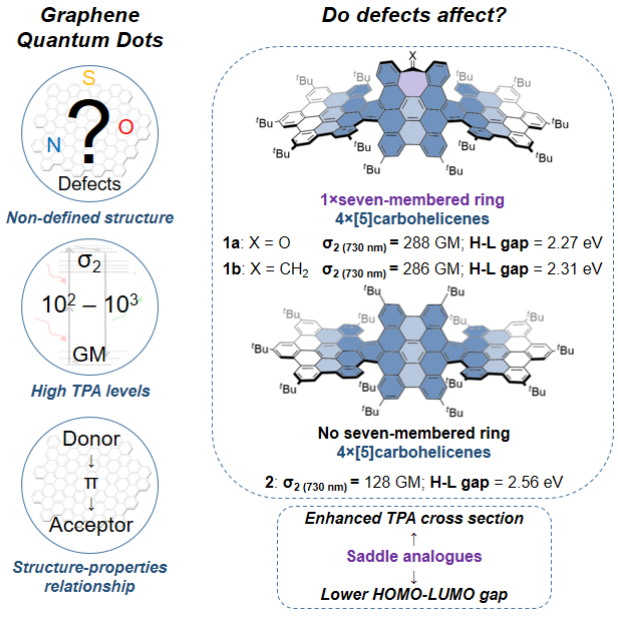

Figure 1. Background and optical and electrochemical features of nanographenes **1a**, **1b** and **2** (*P,P,M,M* enantiomers are shown).

Our group has been working on the design of nanographene-type chromophores potentially applicable in optoelectronics. We have synthesized different sized and shaped nanographene ribbons.

[a] Dr. Silvia Castro-Fernández, Carlos M. Cruz, Dr. Irene R. Márquez, Vicente G. Jiménez, Lucía Palomino-Ruiz, Prof. Juan M. Cuerva, and Dr. Araceli G. Campaña
Departamento de Química Orgánica, Facultad de Ciencias
Unidad de Excelencia Química Aplicada a Biomedicina y Medioambiente. Universidad de Granada. Avda. Fuentenueva, s/n, E-18071 Granada, Spain. E-mail: araceligc@ugr.es

[b] Dr. Inês F. A. Mariz and Dr. E. Maçôas
Centro de Química Estructural and Institute of Nanoscience and Nanotechnology (IN), Instituto Superior Técnico.University of Lisbon
Av. Rovisco Pais, 1, 1049-001 Lisboa, Portugal

¶ Equally contributed to this work

Supporting information for this article is given via a link at the end of the document.

Recently, we described a non-planar ribbon-shaped nanographene constituted by the fusion of both a curved and a planar hexa-*peri*-hexabenzocoronene (HBC) units generating a [5]carbohelicene as frontier between them. The presence of a seven-membered ring at one of the ribbon edges ending in an electron withdrawing ketone functionality resulted in deep saddle-shaped curvature and original optoelectronic properties such as TPA-based upconversion (σ_2 = 130 GM at 760 nm).[11] This prompted us to develop a more complex bent nanographene ribbon formed, in this occasion, by two distorted heptagon-containing HBCs (hept-HBCs) bridged by a planar HBC unit.[12] This disposition of the polyaromatic scaffolds gives place to an undecabenzo[7]helicene (a fully π-extended [7]carbohelicene) and generates two saddle-shaped curved ends, resulting in remarkably higher non-linear optical properties (σ_2 = 870 GM at 800 nm).[13]

As described on the literature, we could observe how the increase of the PAH surface, i.e., the aromatic conjugation, and the increased number of charge-transfer pathways due to the increased number of carbonyl groups, resulted in a marked enhancement of the TPA response.[10a] However, the highest TPA also came out from a more bent PAH bearing two seven-membered rings.[13] There are no systematic studies or evidences about the possible influence of a seven-membered ring intercalated in a polyaromatic system on the TPA response. We wondered if the heptagonal rings have any influence on the TPA rise observed for those ribbon-shaped nanographenes. In such case, NLO properties of graphene-like materials could be modulated by the controlled introduction of saddle-type curvatures that are commonly created by embedding heptagonal carbocycles.[14] In this work, we give answer to that question contributing to the elucidation of the structure-nonlinear optical properties relationships on PAHs through the synthesis of a new family of well-defined distorted nanographene ribbons.

Based on both the literature and our own previous results, we decided to use a new ribbon-shaped PAH constituted by the fusion of three HBC-type scaffolds as aromatic backbone (Fig. 1, bottom). This would give us the desired large conjugated π-surface, appropriate for the multiphoton absorption capability. On the other side, we have previously succeeded on including *t*Bu groups as bulky substituents to force the bending of the polyaromatic surface by the creation of [5]carbohelicene edges. This provides both high solubility in organic solvents and potential chirality for further application. Therefore, in order to get the desired information about the influence of the saddle-shaped curvature, we designed the three derivatives **1a**, **1b** and **2** (Fig. 1, bottom). We included a seven-membered ring in the central HBC unit with (**1a**) and without (**1b**) a EWG ketone functionality and we planned to compare these structures with the third member of the study which does not include the intriguing seven-membered ring (**2**). Comparison between the properties exhibited by **1b** and **2** would give us clear structure-property relationships as **1b** can be consider a good all-carbon heptagon-containing and fully conjugated analogue to **2**.

The synthetic route for the designed nanographene family is shown in Scheme 1. In the case of heptagon-containing PAHs (**1a, b**) we took advantage of our previously developed strategy to easily prepare functionalized saddle-shaped HBC analogues.[13] In this case, heptagon-containing HBC **3** already bears two aryl bromides for further expansion of the PAH (see SI for further details on the synthesis of **3**). Thus, **3** is subjected to a double Sonogashira coupling with 4-*tert*-butylphenylacetylene to give intermediate **4** which after double Diels-Alder reaction with 2,3,4,5-*tetrakis*-(*p*-*tert*-butyl-phenyl)-cyclopentadienone gives precursor **5**. Compound **1a** is obtained by means of a Scholl-type cyclodehydrogenation reaction using the oxidant-acid system DDQ/CF_3SO_3H, which had been proved to be efficient for this sort of distorted polycyclic aromatic systems.

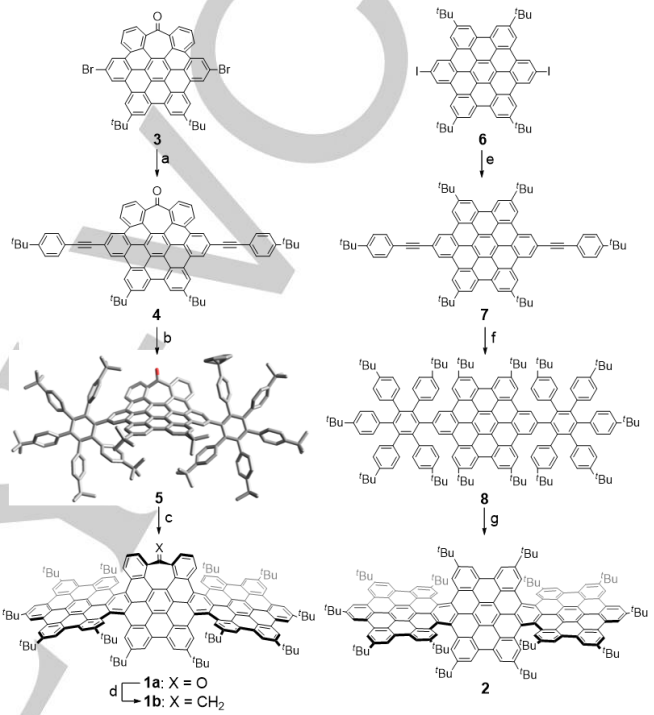

Scheme 1. Synthesis of compounds **1a**, **1b** and **2**. Reagents and conditions: a) 4-*tert*-butylphenylacetylene, $Pd(PPh_3)_4$, CuI, NEt_3, THF, 70°C, 16 h, 76%; b) 2,3,4,5-*tetrakis*-(*p*-*tert*-butyl-phenyl)-cyclopentadienone, Ph_2O, reflux, 8 h, 45 %; c) DDQ, CF_3SO_3H, CH_2Cl_2, 0°C, 10 min, 33%; d) Tebbe's reagent, THF, 0°C to RT, 3 h, 80%; e) 4-*tert*-butylphenylacetylene, $PdCl_2(PPh_3)_2$, CuI, NEt_3, toluene, 60°C, 16 h, 75%; f) 2,3,4,5-*tetrakis*-(*p*-*tert*-butyl-phenyl)-cyclopentadienone, Ph_2O, reflux, 16 h, 29%; g) DDQ, CF_3SO_3H, CH_2Cl_2, 0°C to RT, 10 min, 29%. (*P,P,M,M)* enantiomers are shown. Single crystal X-ray structure of **5** is shown.

The presence of the ketone moiety at the edge of the central heptagonal ring constitutes a key point of this structure, not only because its electron-withdrawing character is expected to favor the TPA response, but also because it enables derivatization that allow us to compare the properties of this structure with similar analogues bearing different functional groups. In this case, we decided to simply remove the oxygen atom, in order to eliminate the electron-withdrawing character of such functionalization with the minimal modification of the whole structure. For this purpose, we subjected **1a** to Tebbe's olefination obtaining **1b** bearing an exocyclic double bond.

For the heptagon free derivative, we prepared difunctionalized HBC **6**, following literature procedures (see SI for details) and we performed an analogue synthetic path (Scheme 1, right). Starting

from **6**, first a double Sonogashira coupling reaction with 4-*tert*-butylphenylacetylene to obtain compound **7**. Then, the aromatic network is expanded by means of a two-fold Diels-Alder reaction with 2,3,4,5-tetrakis-(*p*-*tert*-butyl-phenyl)-cyclopentadienone giving precursor **8**, which after cyclodehydrogenation with DDQ/CF_3SO_3H gave compound **2**, the third member of the study. The presence of bulky ^{t}Bu groups as lateral chains gives place to four [5]carbohelicenes between the central and the lateral HBC units, which depending on their chirality would determine the symmetry of the final ribbon. At first, it was expected to obtain a mixture of several diastereoisomers, with the corresponding enantiomers in the case of those which would be chiral. However, when observing the ^{1}H-NMR spectrum of compound **1a**, we found that an unexpected simple spectrum was obtained (Fig. 2, **1a**) suggesting the formation of a symmetric compound with only six ^{t}Bu groups proton signals and the signals characteristic of the aromatic rings besides the central heptagon (two doublets and a triplet). High-resolution mass spectrometry (HRMS, ESI-TOF) confirmed the isolation of **1a** (Fig. S32). Subsequent HPLC analysis (in both normal and chiral stationary phase) indicated that only one *meso* diastereoisomer had been formed. In order to elucidate the configuration of the final compound we proceeded with the theoretical optimization (DFT-CAMB3LYP/6-31G(d,p)) of the two possible achiral *meso* diastereoisomers, (*P,P,M,M*)-**1a** (Fig. 3, left) and (*P,M,P,M*)-**1a** (Fig. 3, right). Comparison of the relative stabilities of (*P,P,M,M*) and (*P,M,P,M*) diastereoisomers of **1a**, suggested (*P,P,M,M*)-**1a** to be *ca.* 5 kcal mol^{-1} more stable than (*P,M,P,M*)-**1a**. Considering that the absence of ^{t}Bu groups at the edges of [5]helicenes created around the tropone moiety should result in an easily surmountable isomerization barrier, the idea of finally obtaining only the most stable diastereoisomer is consistent with the experimental observation. Finally, the comparison between the experimental and the calculated UV-vis spectra of the two possible achiral diastereoisomers strongly supported that (*P,P,M,M*) would be the only formed configuration (Fig. 3, bottom). This is also in agreement with the resolved X-ray structure of precursor **5** (Scheme 1), where the lateral *pentakis*(4-*tert*-butylphenyl)benzene units present a crossed-like arrangement respect to the central saddle-HBC in a symmetric manner as in the (*P,P,M,M*)-**1a** diastereoisomer.

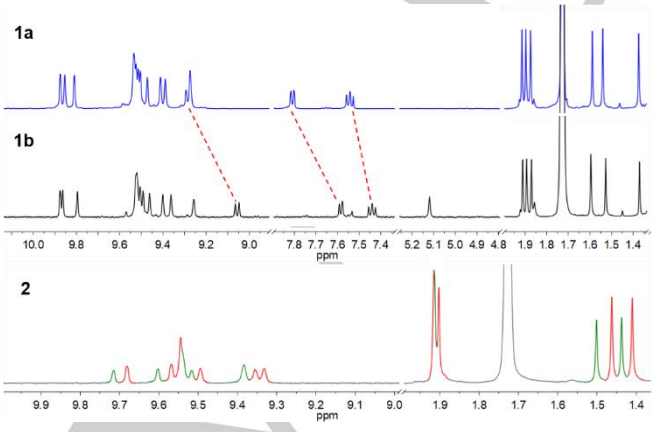

Figure 2. Stack plot of partial ^{1}H NMR spectra of compounds **1a**, **1b** and **2** (first diastereoisomer signals in red (57%), diastereoisomer signals in green (43%)) (500 MHz, C_4D_8O). Aromatic signals have a magnification factor of 3×.

As expected, the ^{1}H-NMR spectrum of **1b**, presented few differences respect to that of **1a**, being the most appreciable ones the shifting upfield of the triplet and doublets corresponding to the protons of the aromatic ring besides the heptagon and the appearance of the diagnostic signal of the exocyclic double bond protons at 5.1 ppm (Fig. 2, middle). This is in agreement with the change of the electron withdrawing carbonyl group by an exocyclic double bond. The other proton signals barely change, as expected, because of being obtained by derivatization of **1a** and, therefore, pointing also to a single symmetric diastereoisomer.

In the case of the totally hexagonal analogue **2**, a mixture of diastereoisomers was obtained manifesting as two sets of ^{t}Bu groups signals at the ^{1}H-NMR spectrum in a 1.3 to 1 ratio (Fig. 2, bottom). HPLC separation led to two diastereoisomers with practically identical UV-vis spectra and ^{1}H-NMR signals (Fig. S27-S31) which summed the one of the previous mixture. Considering that in compound **2** the central HBC is connected by the two lateral HBCs by four [5]carbohelicenes with bulky ^{t}Bu groups at both the edges of all of them (Fig. 1), it could be expected the isomerization barrier here to be higher, hindering the isomerization and making possible to separate them.

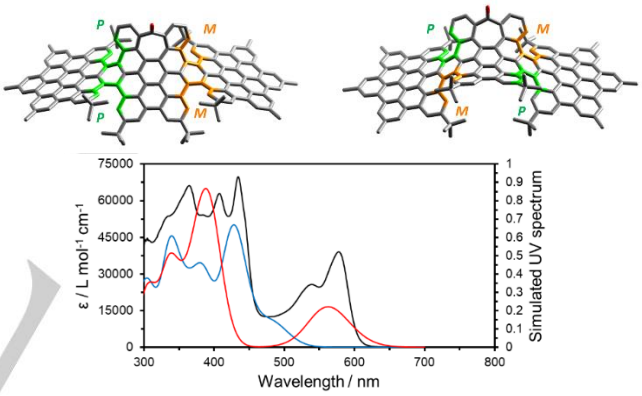

Figure 3. Top: DFT-CAMB3LYP/6-31G(d,p) optimized structures of (*P,P,M,M*)-**1a** (left) and (*P,M,P,M*)-**1a** (right); Bottom: Comparison between experimental UV-vis spectrum of **1a** (black) and calculated UV-vis spectra for (*P,P,M,M*)-**1a** (red), (*P,M,P,M*)-**1a** (blue).

Once the structure of the three new ribbon-type nanographenes was well-defined, we proceeded with the study of their photophysical properties in order to draw the expected structure-optical properties relationships. We found similar one-photon absorption (OPA) spectra shapes for all of them and significant differences in their intensities (Fig. 4).

Compounds **1a** and **1b** have stronger OPA, with maximum molar absorptivity (ε) of 7.0x10^4 M^{-1} cm^{-1} at 434 nm and 8.2x10^4 M^{-1} cm^{-1} at 433 nm, respectively. Compound **2** has a considerably less intense OPA response, with maximum molar absorptivity of 4.0x10^4 M^{-1}cm^{-1} at 443 nm, which is half of that of the seven-membered ring containing analogues. Also, they all present an intense red-shifted absorption band corresponding to the lowest energy transition centered at 578 nm (3.9x10^4 M^{-1}cm^{-1}), 577 nm (4.7x10^4 M^{-1}cm^{-1}) and 575 nm (1.9x10^4 M^{-1}cm^{-1}) for **1a**, **1b** and **2**, respectively. The three compounds present intense one-photon

emission (OPE) bands with nearly coincident wavelength maxima at 594, 598 and 594 nm, for **1a**, **1b** and **2**, respectively. The emission quantum yields (LQY) are generally high, slightly higher in the case of the seven-membered ring containing nanoribbons, 71 % for **1a**, 76 % for **1b** and 69 % for **2**. Despite the similarity on the OPA and OPE spectra profiles, the OPA brightness (ε x LQY) are significantly higher for the seven-membered ring containing compounds, *ca.* twice higher, than for the totally hexagonal analogue.

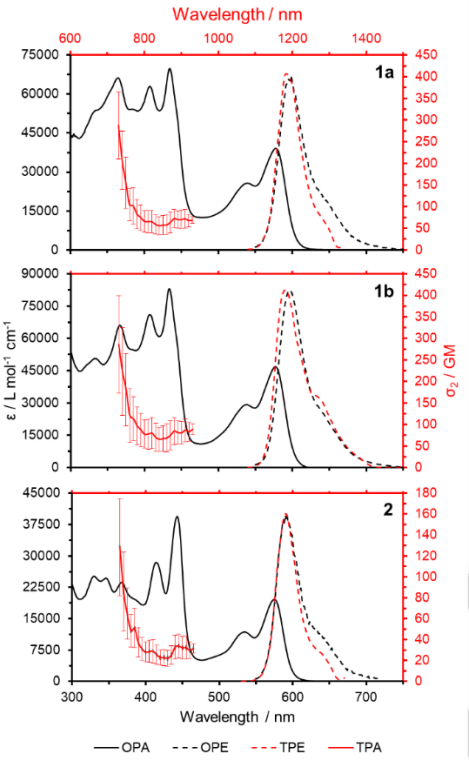

Figure 4. One-photon absorption (OPA), two-photon absorption (TPA), one-photon emission (OPE) and two-photon emission (TPE) spectra of compounds **1a** (λ_{exc} = 500 nm), **1b** (λ_{exc} = 548 nm) and **2** (λ_{exc} = 500 nm) measured at approximately 10^{-6} M in CH_2Cl_2. The TPA data is shown in the secondary red axis.

The NLO excitation spectra of compounds **1a**, **1b** and **2** were recorded in the 710-950 nm range and the absorption cross-section estimated using the two-photon induced fluorescence method as detailed in the SI (Fig. 4, Fig. S44). For all compounds, the TPA cross-section maximum measured at 730 nm was 288 GM, 286 GM and 128 GM, respectively for **1a**, **1b** and **2**. It was expected that the presence of the carbonyl group increased the TPA response of **1a**, with respect to **2**, since its electron withdrawing character could affect charge transfer character of the electronic transitions. However, the all-carbon analogue **1b**, without the ketone moiety still showed a TPA cross-section of practically the same value than **1a**, which in both cases is twice than that of compound **2**. The slight difference between **1a** and **1b** can be understood considering that the effect of the electron withdrawing power of a single carbonyl compound placed in the middle of the molecule is not so relevant when compared with the conjugation length of the nanoribbons. On the other hand, the fact that the seven-membered ring analogues have a two-fold increase in the TPA cross-section when compared with compound **2** does points to the heptagon unit as being determinant in the nonlinear response of the nanographenes. This implies that the saddle-shaped curvature created by the presence of the seven-membered ring definitively affects the TPA capability of the nanographene ribbon, strongly increasing its cross section value.

Additionally, the electrochemical analysis using both cyclic and square wave voltammetries of **1a**, **1b** and **2** showed, at least, two oxidation potentials and more than five reduction potentials for all of them and pointed out how easily the HOMO-LUMO gap can be tuned by the functionality of the PAH surface (See Figure S46). Compound **2** presents larger HOMO-LUMO gap (2.56 eV) compared to those of the seven-membered ring containing nanographenes **1a** and **1b**, with slightly short HOMO-LUMO gap for the first one, as expected due to the presence of the ketone moiety (2.27 eV for **1a** vs. 2.31 eV for **1b**). These results indicate that the saddle-shaped curvature has also a clear effect on the energy gap of these nanographenes, decreasing its HOMO-LUMO gap in *ca.* 10% (from 2.56 eV for **2** to 2.31 for all-carbon **1b**).

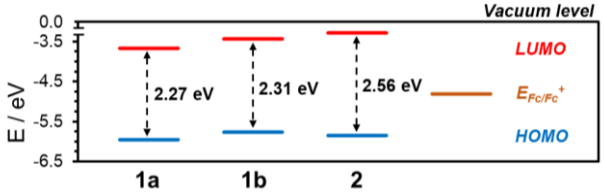

Figure 5. Schematic diagram illustrating the energies of the HOMO and LUMO levels and the corresponding electrochemical gap in compounds **1a**, **1b** and **2** referenced to the vacuum level ($E_{Fc/Fc+}$ = -4.80 eV).

In conclusion, we have demonstrated the relevance of the seven-membered rings among all the defects that contribute to exploit the outstanding properties of graphene by disturbing its pristine structure. We have found that the saddle-shaped curvature created by this odd-membered ring improves the NLO response of nanographene ribbons, doubling the TPA cross section in comparison with a purely hexagonal analogue PAH. Furthermore, we have shown that the saddle-shaped curvature has also a clear effect diminishing the energy gap of similar size nanographenes. These results show that the preparation of well-defined graphene molecules with novel curvatures and distortions and the establishment of unequivocal structure-property relationships become mandatory for their future application. We reinforced the idea that introducing distortions on nanographenes, in a well-defined manner, is a viable molecular engineering strategy to fit their properties for optoelectronic devices.

Acknowledgements

We acknowledge the European Research Council (ERC) under the European Union's Horizon 2020 research and innovation

program (ERC-2015-STG-677023) and the Spanish Ministerio de Ciencia Innovación y Universidades (PGC2018-101181-B-I00) and Ministerio de Economía y Competitividad (BES-2016-076371 and RyC-2013-12943). E.M. thanks the Fundação para a Ciência e a tecnologia (PTDC/NAN-MAT729317/2017 and PTDC/QUI-QFI/29319/2017). We thank the CSIRC-Alhambra from the University of Granada.

Keywords: nanostructures • helicenes • nanographenes• nonlinear optics • graphene

[1] A. Narita, X-Y. Wang, X. Feng, K. Müllen, *Chem. Soc. Rev.* **2015**, *44*, 6616−6643.

[2] a) Y. Hu, D. Wang, M. Baumgarten, D. Schollmeyer, K. Müllen, A. Narita, *Chem. Commun.* **2018**, *54*, 13575–13578; b) J. M. Fernández-García, P. J. Evans, S. M. Rivero, I. Fernández, D. García-Fresnadillo, J. Perles, J. Casado, N. Martín, *J. Am. Chem. Soc.* **2018**, *140*, 17188−17196; c) D. Meng, G.Liu, C. Xiao, Y. Shi, L. Zhang, L. Jiang, K. K. Baldridge, Y. Li, J. S. Siegel, Z. Wang *J. Am. Chem. Soc.* **2019**, *141*, 5402−5408; d) M. Navakouski, H. Zhylitskaya, P. J. Chmielewski, T. Lis, J. Cybińska, M. Stępień, *Angew. Chem. Int. Ed.* **2019**, *58*, 4929–4933; *Angew.Chem.* **2019**,*131*,4983–4987; e) Y. Zhu, X. Guo, Y. Li, J. Wang, *J. Am. Chem. Soc.* **2019**, *141*, 5511−5517; f) J. M. Fernández-García, P. J. Evans, S. Filippone, M. Á. Herranz, N. Martín, *Acc. Chem. Res.* **2019**, *52*, 1565−1574. Y. Zhong, B. Kumar, S. Oh, M. T. Trinh, Y. Wu, K. Elbert, P. Li, X. Zhu, S. Xiao, F. Ng, M. L. Steigerwald, C. Nuckolls, *J. Am. Chem. Soc.* **2014**, *136*, 8122–8130.

[3] A. Eftekhari, H. Garcia, *Mater. Today Chem.* **2017**, *4*, 1–16.

[4] a) P. Zheng, N. Wu, *Chem. Asian J.* **2017**,*12*, 2343 –2353; b) R. Gui, H. Jin, Z. Wang, L. Tan, *Coordination Chemistry Reviews* **2017**, *338*, 141–185; c) X. Liu, S.-Y. Chen, Q. Chen, X. Yao, M. Gelléri, S. Ritz, S. Kumar, C. Cremer, K. Landfester, K. Müllen, S. Parekh, A. Narita, M. Bonn, *Angew. Chem. Int. Ed.* **2019**, DOI: 10.1002/anie.201909220; *Angew. Chem.* **2019** 10.1002/ange.201909220; d) L. Li, G. Wu, G. Yang, J. Peng, J. Zhao, J. J. Zhu, *Nanoscale* **2013**, *5*, 4015–4039.; L. Wang, Y. Wang, T. Xu, H. Liao, C. Yao, Y. Liu, Z. Li, Z. Chen, D. Pan, L. Sun, M. Wu, *Nat. Commun.* **2014**, *5*, 5357; e) H. Lu, W. Li, H. Dong, M. Wei, *Small* **2019**, *15*, 1902136; H. Wang, C. Ciret, C. Cassagne, G. Boudebs, *Opt. Mater. Express* **2019**, *9*, 339–351.

[5] a) Q. Liu, B. Guo, Z. Rao, B. Zhang, J. R. Gong, *Nano Lett.* **2013**, *13*, 2436–2441; b) A. Ananthanarayanan, Y. Wang, P. Routh, M. Alam Sk, A. Than, M Lin, J. Zhang, J.Chen, H. Sun, P. Chen, *Nanoscale* **2015**, *7*, 8159–8165; c) S. Lu, G. Xiao, L. Sui, T. Feng, X. Yong, S. Zhu, B. Li, Z. Liu, B. Zou, . M. Jin, J. S. Tse, H. Yan, B. Yang, *Angew. Chem. Int. Ed.* **2017**, *56*, 6187–6191; *Angew.Chem.* **2017**, *129*, 6283–6287; d) S. Lu, L. Sui, J. Liu, S. Zhu, A. Chen, M. Jin, B. Yang, *Adv. Mater.* **2017**, *29,* 1603443.

[6] a) S. Zhu, Y. Song, X. Zhao, J. Shao, J. Zhang, B. Yang, *Nano Res.* **2015**, *8*, 355–381; b) Z. Gan, H. Xu, Y. Hao, *Nanoscale* **2016**, *8*, 7794–7807; c) Noor-Ul-Ain, M.O. Eriksson, S. Schmidt, M. Asghar, P.-C. Lin, P. O. Holtz, M. Syväjärvi, G. R. Yazdi, *Nanomaterials* **2016**, *6*, 198–210; d) C. Santos, I. Mariz, S. Pinto, G. Gonçalves, I. Bidkin, P. Marques, M. Neves, J. Martinho, E. Maçôas, *Nanoscale* **2018**, *10*, 12505–12514; e) K. Yamato, R. Sekiya, S. Nishitani, T. Haino, *Chem. Asian. J.* **2019**, *14*, 3213–3220.

[7] G. S. He, L.-S. Tan, Q. Zheng, P. N. Prasad, *Chem. Rev.* **2008**, *108*, 1245–1330.

[8] For TPA-structure relationship see: a) M. Rumi, J. E. Ehrlich, A. A. Heikal, J. W. Perry, S. Barlow, Z. Hu, D. McCord-Maughon, T. C. Parker, H. Röckel, S. Thayumanavan, S. R. Marder, D. Beljonne, J.-L. Brédas, *J. Am. Chem. Soc.* **2000**, *122*, 9500–9510; b) G. Li, S. Wang, S. Yang, G. Liu, P. Hao, Y. Zheng, G. Long, D. Li, Y. Zhang, W. Yang, L. Xu, W. Gao, Q. Zhang, G. Cui, B. Tang, *Chem. Asian J.* **2019**, *14,* 1807–1813; For TPA-substituents relationship on nanographenes see: c) Z. Zeng, Z. Guan, Q.-H. Xu, J. Wu, *Chem. Eur. J.* **2011**, *17*, 3837–3841; d) R. Yamaguchi, S. Ito, B. S. Lee, S. Hiroto, D. Kim, H. Shinokubo, *Chem. Asian J.* **2013**, *8*, 178–190; For structure-properties relationship on nanographenes see: e) M. M. Martin, D. Lungerich, P. Haines, F. Hampel, N. Jux, *Angew. Chem. Int. Ed.* **2019**, *58*, 8932–8937; *Angew. Chem*. **2019**, *131*, 9027–9032; f) T. Umeyama, T. Hanaoka, H. Yamada, Y. Namura, S. Mizuno, T. Ohara, J. Baek, J. Park, Y. Takano, K. Stranius, N. V. Tkachenko, H. Imahori, *Chem. Sci.* **2019**, *10*, 6642–6650.

[9] a) J.-F. Nicoud, F. Bolze, X.-H. Sun, A. Hayek, P. Baldeck, *Inorg. Chem.* **2011**, *50*, 4272–4278; b) H. M. Kim, B. R. Cho, *Chem. Rev.* **2015**, *115*, 5014–5055; c) D. Li, X. Tian, A. Wang, L. Guan, J. Zheng, F. Li, S. Li, H. Zhou, J. Wu, Y. Tian, *Chem. Sci.* **2016**, *7*, 2257–2263; d) C. M. Jimenez, D. Aggad, J. G. Croissant, K. Tresfield, D. Laurencin, D. Berthomieu, N. Cubedo, M. Rossel, S. Alsaiari, D. H. Anjum, R. Sou grat, M. A. Roldan-Gutierrez, S. Richeter, E. Oliviero, L. Raehm, C. Charnay, X. Cattoën, S. Clément, M. W. C. Man, M. Maynadier, V. Chaleix, V. Sol, M. Garcia, M. Gary-Bobo, N. M. Khashab, N. Bettache, J.-O. Durand, *Adv. Funct. Mater.* **2018**, *28*, 1800235; e) C. Zhang, Y. Zhao, D. Li, J. Liu, H. Han, D. He, X. Tian, S. Li, J. Wub, Y. Tian, *Chem. Commun.* **2019**, *55*, 1450–1453. For other possible and less explored recent applications see for example: f) R. A. Jensen, I-C. Huang, O. Chen, J. T. Choy, T. S. Bischof, M. Lončar, M. G. Bawendi, *ACS Photonics* **2016**, *3*, 423–427; g) I. Carmi, M. Battista, L. Maddalena, E. C. Carroll, M. A. Kienzler, S. Berlin, *Nat. Protoc.* **2019**, *14*, 864–900.

[10] a) F. Terenziani, C. Katan, E. Badaeva, S. Tretiak, M. Blanchard-Desce, *Adv. Mater.* **2008**, *20*, 4641–4678; b) D. Li , B. Li, S. Wan, C. Zhang, H. Cao, X. Tian, Y. Tian, *Spectrochim. Acta A* **2020**, *224*, 117448.

[11] C. M. Cruz, I. R. Márquez, I. F. A. Mariz, V. Blanco, C. Sánchez-Sánchez, J. M. Sobrado, J. A. Martín-Gago, J. M. Cuerva, E. Maçôas, A. G. Campaña, *Chem. Sci.* **2018**, *9*, 3917−3924.

[12] I. R. Márquez, N. Fuentes, C. M. Cruz, V. Puente-Muñoz, L. Sotorrios, M. L. Marcos, D. Choquesillo-Lazarte, B. Biel, L. Crovetto, E. Gómez-Bengoa, M. T. González, R. Martin, J. M. Cuerva, A. G. Campaña, *Chem. Sci.* **2017**, *8*, 1068−1074.

[13] C. M. Cruz, S. Castro-Fernández, E. Maçôas, J. M. Cuerva, A. G. Campaña, *Angew. Chem. Int. Ed.* **2018**, *57*, 14782−14786; *Angew. Chem.* **2018**, *130*,14998–15002.

[14] a) I. R. Márquez, S. Castro-Fernández, A. Millán, A. G. Campaña, *Chem. Commun.* **2018**, *54*, 6705−6718; b) S. H. Pun, Q. Miao, *Acc. Chem. Res.* **2018**, *51*, 1630−1642.

Entry for the Table of Contents

COMMUNICATION

The advantage of defects: the effect of a saddle curvature on the nonlinear optical properties of ribbon-shaped nanographenes is unequivocally demonstrated. Curved edges created by the inclusion of heptagonal carbocycles enhance the two-photon absorption on graphene molecules.

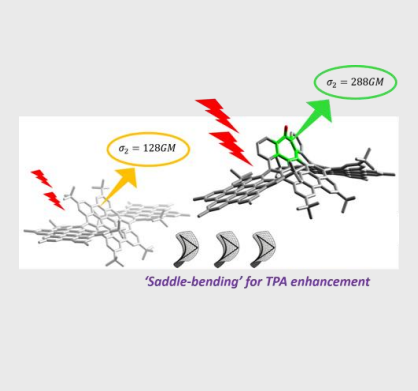

Silvia Castro-Fernández, Carlos M. Cruz, Inês F. A. Mariz, Irene R. Márquez, Vicente G. Jiménez, Lucía Palomino-Ruiz, Juan M. Cuerva, Ermelinda Maçôas and Araceli G. Campaña**

1 – 5

Two-photon absorption enhancement by the inclusion of saddle curvature in distorted nanographene ribbons